Normal-state optical properties of $Nd_{1.85}Ce_{0.15}CuO_{4+\delta}$

R. A. Hughes, Y. Lu, and T. Timusk
Institute for Materials Research, McMaster University, Hamilton, Ontario, Canada L8S 4M1

J. S. Preston
Department of Engineering Physics, McMaster University, Hamilton, Ontario, Canada L8S 4M1
(Received 14 May 1992)

We present a detailed temperature dependence of the far-infrared reflectance for $Nd_{1.85}Ce_{0.15}CuO_{4+\delta}$ films grown by pulsed-laser deposition. The reflectance spectra clearly show the presence of a ledge at 420 cm^{-1} offering further evidence that this feature is common to all the cuprate superconductors. The optical conductivity obtained from Kramers-Kronig analysis can be divided into two components. The first component, which is strongly temperature dependent, is fit to a Drude model. This fit indicates that $Nd_{1.85}Ce_{0.15}CuO_{4+\delta}$ has a constant plasma frequency and a temperature-dependent scattering rate that closely follows the temperature dependence exhibited by the dc resistivity. The second component shows little temperature dependence and is described by a model that couples phonons to a midinfrared band. Comparisons between the optical conductivity and the structures seen by tunneling and inelastic-neutron-scattering measurements are made.

I. INTRODUCTION

Among the cuprate superconductors $Nd_{2-x}Ce_xCuO_{4+\delta}$ is unique. It is a high-temperature superconductor that allows the CuO_2 planes to be doped with electrons rather than holes.[1,2] The dc resistivity exhibits a T^2-like temperature dependence[3] rather than the more common linear behavior. The superconducting transition temperature, which never exceeds 23 K and is strongly dependent upon both the cerium and oxygen concentrations, is low compared to the other cuprates. Its crystal structure lacks the apical oxygen atoms which makes its CuO_2 planes structurally more two dimensional than any other high-temperature superconductor. These unique transport and structural properties make $Nd_{2-x}Ce_xCuO_{4+\delta}$ an attractive candidate for detailed investigations of its optical properties. These investigations will allow direct comparisons to the more well-established cuprate superconductors to determine if the unique properties displayed by $Nd_{2-x}Ce_xCuO_{4+\delta}$ manifest themselves in the optical spectra.

Most of the optical investigations performed on $Nd_{2-x}Ce_xCuO_{4+\delta}$ single crystals have focused upon the effects of adding electrons to the CuO_2 planes through the substitution of Ce^{4+} on the Nd^{3+} site.[4-8] These measurements clearly show the development of the midinfrared band as carriers are added to the CuO_2 planes. This is accompanied by a decrease in the oscillator strength for the energies above 1.5 eV which are associated with a charge-transfer band. This behavior is very reminiscent of that obtained for the $La_{2-x}Sr_xCuO_4$ compound as the number of holes is varied by adjusting the value of x.[9] For cerium concentrations in excess of the optimum for superconductivity, typically $x \approx 0.2$, the spectra become more Drude-like and the reflectance becomes more metallic.

The optical work presented here will focus on the temperature dependence of the *ab* plane optical conductivity at low frequency. Samples with oxygen and cerium concentrations that give the optimum T_c were used. They will be used in a detailed investigation of the temperature dependence of the far-infrared reflectance to gain insight into the normal-state excitation spectrum.

II. EXPERIMENT

The reflectance measurements were performed on $Nd_{1.85}Ce_{0.15}CuO_{4+\delta}$ thin films deposited by laser deposition. Pulses from an excimer laser ($\lambda = 308\eta m$, fluence = 2 J/cm^2) were focused onto a stoichiometric polycrystalline pellet. The substrate used was (100) $SrTiO_3$ as it has a close lattice match to $Nd_{1.85}Ce_{0.15}CuO_{4+\delta}$ (mismatch = 1.03%) and is suitable for epitaxial growth with the *c* axis of the film perpendicular to the substrate. During the deposition the substrate was held at a temperature of 780 °C in oxygen at a pressure of 300 mtorr. Superconducting films can only be made by carefully controlling the oxygen stoichiometry through high-temperature vacuum anneals as a small excess of oxygen can render the sample nonsuperconducting. A 4-h anneal at a temperature of 600 °C was sufficient to obtain a superconductor with a transition temperature onset at 21 K and a width of 1.5 K (Fig. 1). Annealing temperatures which are this low are only viable for films as their large surface area to volume ratio provides optimal conditions for the reduction process. Vacuum anneals at higher temperatures result in films with copper-deficient surfaces. The details of the film growth will be published elsewhere.[10]

The room-temperature midinfrared (1000–5000 cm^{-1}) optical properties of all the films produced were exam-

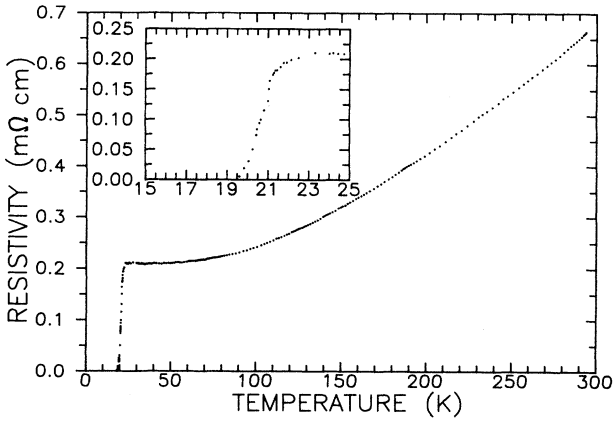

FIG. 1. Resistivity vs temperature for a $Nd_{1.85}Ce_{0.15}CuO_{4+\delta}$ film deposited on (100) $SrTiO_3$ by pulsed-laser deposition. The inset shows the superconducting transition which onsets at a temperature of 21 K and has a width of 1.5 K.

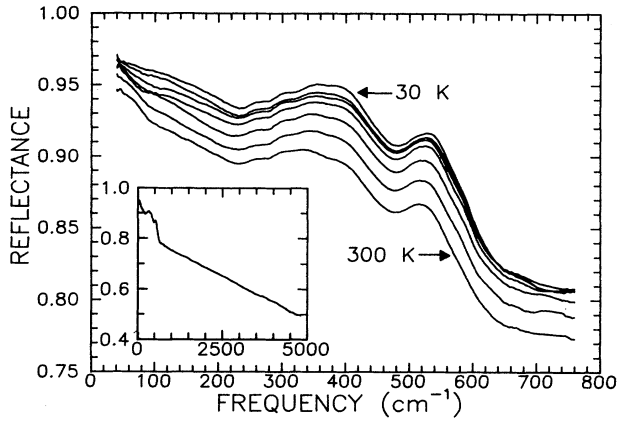

FIG. 2. Reflectance vs frequency for a $Nd_{1.85}Ce_{0.15}CuO_{4+\delta}$ sample. The spectra taken at 30 and 300 K are labeled on the graph. The intermediate spectra are for temperatures at 100, 125, 150, 200, and 250, whereby there exists a systematic increase in the reflectance as the temperature is lowered. Measurements were also made at 60, 175, 225, and 275 K, but they have been excluded for the sake of clarity. The inset shows that the room-temperature reflectance has a linear dependence at midinfrared frequencies.

ined using a Spectra-Tech infrared microscope. Only those samples which displayed a reflectance which was both high and homogeneous over the entire film surface were used for detailed optical investigations. Single bounce far-infrared reflectance measurements were performed using a rapid scan interferometer. Focused optics directed the light onto the sample located in a continuous flow cold finger cryostat. Temperatures as low as 15 K could be reached. The absolute value of the reflectance was determined by an *in situ* evaporation of gold onto the sample. By remeasuring the reflectance of the coated sample, geometrical differences between the sample and reference mirror were taken into account.

III. RESULTS

The optical properties of five superconducting $Nd_{1.85}Ce_{0.15}CuO_{4+\delta}$ thin films have been examined. All of the samples show similar behavior. Thus, in this report we will concentrate on the optical properties of a single sample where an extensive temperature-dependent study was undertaken. Figure 2 shows the normal-state reflectance as a function of temperature. The sample exhibits a systematic increase in the reflectance as the temperature is lowered where, on average, the extent of the change becomes smaller at low temperatures. The magnitude of the reflectance at low frequencies is quite high and is comparable to that of $YBa_2Cu_3O_{7-\delta}$. Three distinct features appear in the spectrum; a reflectance minimum at 230 cm^{-1} and the reflectance ledges at 420 and 540 cm^{-1}. The first 420-cm^{-1} ledge has been demonstrated to be a common feature for the cuprate superconductors. It is very prominent in the reflectance spectrum of the $Bi_2Sr_2CaCu_2O_8$,[11] $Tl_2Ba_2CaCu_2O_8$,[12] and $Pb_2Sr_2(Y/Ca)Cu_3O_x$ (Ref. 13) superconductors. The ledge is also present in $YBa_2Cu_3O_{7-\delta}$,[14] but it is often obscured by the high reflectance associated with the free electrons and only becomes evident as the sample becomes superconducting. The appearance of this ledge in $Nd_{1.85}Ce_{0.15}CuO_{4+\delta}$ with a T_c of 21 K and in $Tl_2Ba_2CaCu_2O_8$ with a T_c of 100 K (Ref. 12) clearly indicates that it is associated with the normal-state excitation spectrum and is independent of superconducting transition temperature. As in all the other cuprates, the midinfrared reflectance shows a non-Drude behavior. The inset of Fig. 2 shows the room-temperature reflectance which is linear up to 5000 cm^{-1}. This linear dependence is a feature common to many of the oxide superconductors.[15]

The optical conductivity offers a clearer picture of the normal-state excitation spectrum. It is obtained through the model-independent Kramers-Kronig transformations. This calculation was performed using a Drude extrapolation at low frequencies and high-frequency extrapolations ($\omega \geq 5000$ cm^{-1}) based on the work of Lupi *et al.*[7] and

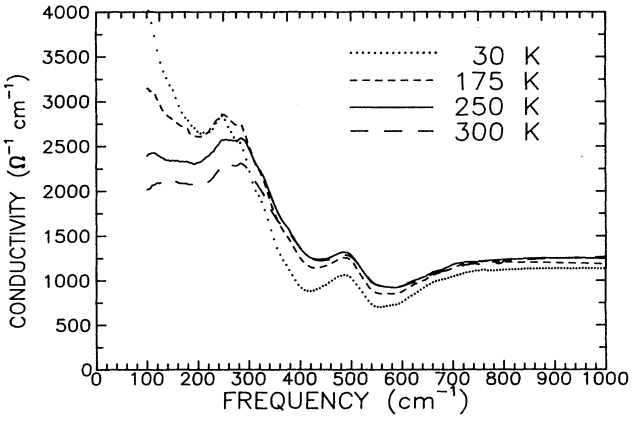

FIG. 3. The conductivity vs frequency for a selected group of temperatures. There is clearly a shift in the spectral weight to lower frequencies as the temperature is lowered. This shift is caused by the narrowing of the Drude peak associated with the reduced scattering rate at lower temperatures.

Tajima *et al.*[16] Figure 3 shows the result of this calculation. The curves clearly illustrate that the spectral weight is shifting towards lower frequencies as the temperature is lowered. This is consistent with a narrowing of the free-carrier Drude peak associated with a reduced scattering rate at low temperatures. At 300 K the Drude peak is barely discernible while at 30 K a well-developed peak centered at zero frequency appears. A fit to the prominent Drude peak displayed by the 30-K data allows its contribution to the total conductivity to be subtracted out leaving behind the features associated with other excitations (see Fig. 4). Apart from the peak centered at 490 cm^{-1}, the result is qualitatively similar to the equivalent plot displayed by $YBa_2Cu_3O_{7-\delta}$. This structure has been described by a model that couples phonons to a midinfrared continuum[17] and it will be used here to fit the data.

The model, which was first developed by Rice[18] for organic superconductors, describes the optical response of a material using the dielectric function given by

$$\epsilon = \left[1 - \frac{\omega_{PD}^2}{\omega^2 + i\omega\Gamma_D}\right] + \frac{\omega_{Pe}^2}{\omega_e^2 - D - \omega^2 - i\omega\Gamma_e} + \epsilon_\infty , \quad (1)$$

where

$$D = \sum_k \frac{\omega_{Pk}^4}{\omega_k^2 - \omega^2 - i\omega\Gamma_k} . \quad (2)$$

The first term describes the free-electron behavior in terms of a simple Drude model which has the plasma frequency (ω_{PD}) and scattering rate (Γ_D) as the adjustable parameters. The second term describes how the midinfrared band with its position (ω_e), strength (ω_{Pe}), and width (Γ_e) is coupled to phonons described in a similar manner by ω_k, ω_{Pk}, and Γ_k. The final term gives the high-frequency dielectric constant (ϵ_∞).

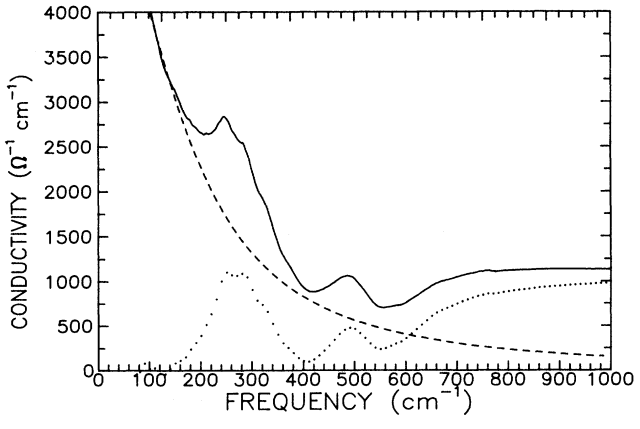

FIG. 4. Subtracting the Drude component (dashed) from the total conductivity (solid) leaves behind structure (dots) which can be described by phonons coupled to an electronic continuum.

The features associated with the electron-phonon interaction in this model can be contrasted with an interpretation of the optical data in terms of Holstein phonon structure. In the Holstein process,[19–21] a charge carrier absorbs a photon and emits a phonon. Both the electron and phonon are needed in the process if momentum and energy are to be conserved. With a coupling constant of the order of unity, large changes are predicted to occur in the Holstein structure when the material becomes superconducting. In particular, the whole phonon structure should become sharper and shift towards higher frequency by 2Δ. In other high-temperature superconductors, the structure in the phonon region changes very little at T_c and has therefore been interpreted not as a Holstein process but in terms of an interference between the continuum electronic absorption and particular phonons giving rise to asymmetric Fano[22] line shapes.[17,23] We shall demonstrate that the distinction between these processes is important for any comparison of optical and tunneling spectra and crucial for any comparison with a direct measurement of the phonon density of states.

The fits of our model to the data indicate that most of the temperature dependence can be accounted for by variations in the Drude term of Eq. (1). Figure 5 shows the values obtained for the scattering rate and the plasma frequency. The plasma frequency is essentially constant, while the temperature dependence of the scattering rate

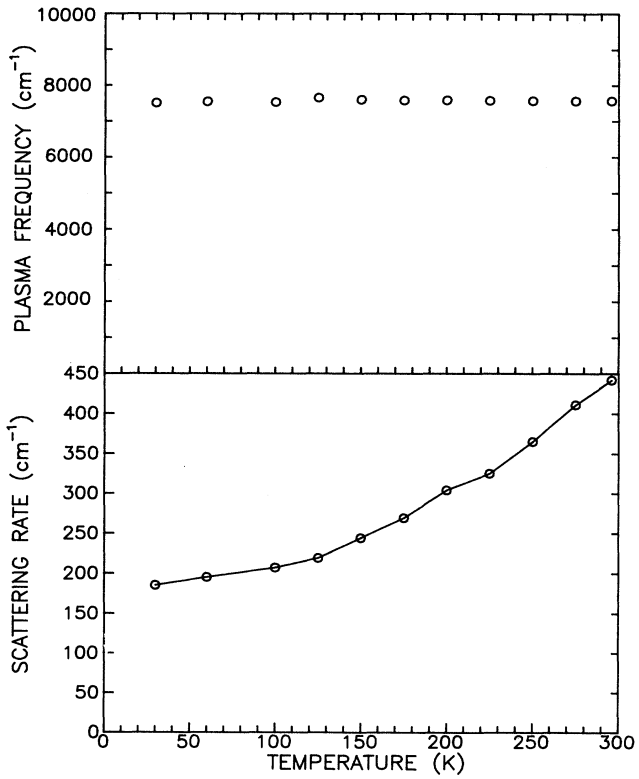

FIG. 5. The plasma frequency and scattering rate as a function of temperature. The plasma frequency is essentially constant while the scattering rate follows a temperature dependence similar to the dc resistivity.

TABLE I. The fitted parameters describing the midinfrared band and the phonons which are coupled to it. All values are in units of cm^{-1}.

	ω_e	ω_{Pe}	Γ_e
Mid-IR band	1870	26 300	10 100
	ω_k	ω_{Pk}	Γ_k
Phonon 1	523	729	46
Phonon 2	415	786	14
Phonon 3	118	564	5

shows a striking resemblance to the dc resistivity. The second term, which describes the coupling between phonons and a broad midinfrared band, has little temperature dependence. There is some sharpening of the structure centered around 270 cm^{-1}, but this is small in comparison to the changes associated with Drude term. The fit requires three phonons that are coupled to the midinfrared band. Table I lists the parameters which describe the fit to the 30-K conductivity data. It is important to note that the phonon frequencies correspond to minima in the conductivity. The implication of these results is that the dc resistivity is solely described by a temperature-dependent free-carrier scattering rate without the need for the dramatic changes to the carrier concentration implied by Hall measurements. This is consistent with the results of Kamarás *et al.*[24] on $YBa_2Cu_3O_{7-\delta}$ and Romero *et al.*[25] on $Bi_2Sr_2CaCu_2O_8$ which show a scattering rate which varies linearly with temperature and intercepts the origin of the scattering rate versus temperature plot.

The parameters obtained from the fits are reasonable. The Drude plasma frequency, which is equal to 0.94 eV, is comparable to the values obtained for all the other oxide superconductors. The scattering rate of 440 cm^{-1} at room temperature is somewhat higher than the values near 300 cm^{-1} obtained for $YBa_2Cu_3O_{7-\delta}$, but this is expected since $Nd_{2-x}Ce_xCuO_{4+\delta}$ has a built-in disorder from the cerium dopant and films have considerably more defects than single crystals. The dc resistivity obtained from these fitted parameters using the simple Drude formula $\rho=4\pi\Gamma_D/\omega_{PD}^2$, shows reasonable agreement with the values obtained from the dc resistivity measurements. At 30 K the agreement is excellent. The measured resistivity is given by 0.21 mΩ cm, compared to a value of 0.19 mΩ cm derived from the optical conductivity. At room temperature the two values differ by 30%.

The partial sum rule for the optical conductivity can be used to calculate the effective number of carriers per formula unit ($N_{\rm eff}$) contributing to the optical properties for frequencies up to ω. It is given by

$$N_{\rm eff}(\omega)=\frac{2mV_{\rm cell}}{\pi e^2}\int_0^{\omega}\sigma(\omega')d\omega' , \tag{3}$$

where V_c is the volume of the unit cell, m_e is the electron mass, and e is the electron charge. Performing this calculation for energies below the charge-transfer band gives $N_{\rm eff}=0.33$ electrons per formula unit. This value is in excellent agreement with the results obtained by Cooper *et al.*[4] on $Pr_{2-x}Ce_xCuO_{4+\delta}$ single crystals. There is also good agreement with the value extracted from the results of Abel *et al.*[8] on $Nd_{2-x}Ce_xCuO_{4+\delta}$, who find a Drude plasma frequency of 1.5 eV significantly larger than the one obtained for these films. It should be noted that $N_{\rm eff}=0.15$ is the expected value if all of this spectral weight is due to the carriers introduced by doping cerium on the neodymium site. This is obviously not the case.

IV. COMPARISONS TO OTHER EXPERIMENTAL TECHNIQUES

Lynn *et al.*[26] have used inelastic neutron scattering to measure the phonon density of states in superconducting $Nd_{1.85}Ce_{0.15}CuO_{4+\delta}$. Their result is shown in Fig. 6. There is a gap in the neutron data in the 180–250 cm^{-1} region due to the presence of a strong crystal-field level. The solid curve indicates the phonon structures predicted by our fits to the optical conductivity. The agreement is excellent. The neutron spectrum gives peak positions at 105, 411, 524 cm^{-1} compared with the optics results which give peak positions at 118, 415, and 523 cm^{-1}. The neutron peak at 766 cm^{-1} does not appear to couple to the electronic continuum, but this feature may also be due to a crystal-field excitation.[26]

It is also worthwhile to compare the infrared spectra with the tunneling measurements of Huang *et al.*[27] on $Nd_{1.85}Ce_{0.15}CuO_{4+\delta}$. These data show a strong resemblance to the I-V curves obtained from a traditional BCS superconductor. A gaplike feature with $2\Delta/k_bT_c=3.9$ is seen and the tunneling conductance exhibits symmetric structure. Superimposed on the smooth BCS-like tunneling conductance is a fine structure in the phonon region. In their straightforward interpretation, the electron-phonon interaction affects the tunneling process and produces the familiar phonon structure proportional to the *derivative* of the tunneling conductance.[28] The same process should give rise to Holstein phonon structure in the optical conductivity[29] which also resembles the derivative of the phonon density of states. In both processes, roughly, a phonon of frequency Ω gives rise to an onset of conductivity at $2\Delta+\hbar\Omega$. Huang *et al.*[27] have used this process to interpret their tunneling data for $Nd_{1.85}Ce_{0.15}CuO_{4+\delta}$. Applying the McMillan-Rowell procedure[30] they find an $\alpha^2F(\Omega)$ from which they calculate a λ of the order of unity and a T_c of 20 K in agreement with the observed transition temperature.

In light of the analysis of Huang *et al.*[27] and our analysis of the optical conductivity we anticipated agreement between the peaks in the $\alpha^2F(\omega)$ function found from the analysis of the tunneling spectrum and minima in the optical conductivity, since both correspond to spectral regions of strong interaction. This agreement is not found. Instead, it is found that the *tunneling conductance* shows a strong likeness to the optical conductivity. Figure 7 shows such a comparison. The tunneling conductance has been divided by the BCS conductance, shifted vertically, and rescaled. The phonon structure in the raw tunneling conductance is only of the order of 1% of the total conductance whereas the structure in the optical

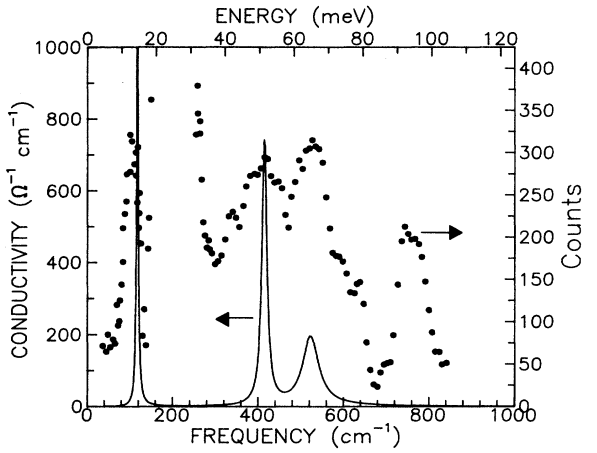

FIG. 6. Comparison of the phonon density of states (dots) derived from inelastic-neutron-scattering experiments (Ref. 23) to the phonon structure predicted by fits to the optical conductivity (solid) (Ref. 23). The gap in the neutron spectrum from 180 to 250 cm^{-1} is due to the interference with a Nd crystal-field transition.

conductance is of the order of 50%. Both energy scales start at zero: zero frequency for the optical conductance and zero bias for the tunneling.

The agreement between the tunneling conductance and the optical conductivity is striking. Roughly equal amplitude minima appear in both curves at 150 and 400 cm^{-1}. A third minimum, seen in the optical data at 580 cm^{-1}, does not appear clearly in the tunneling data. The accuracy at low frequency in both sets of measurements is poorer. In the optical conductivity the rising Drude absorption hides the weak midinfrared band. In the tunneling spectrum the BCS correction becomes larger at low energy.

At this point we do not have a clear understanding

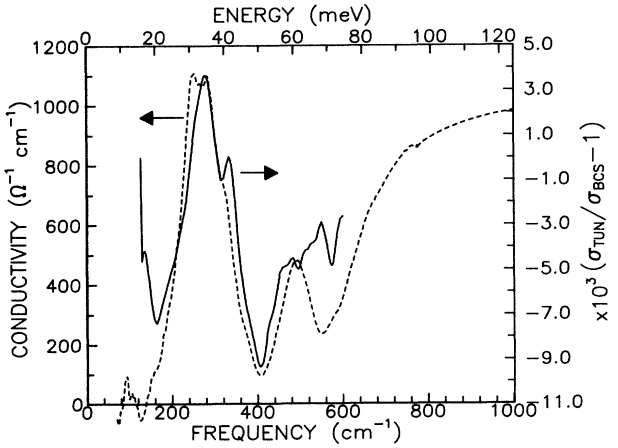

FIG. 7. Comparison of the tunneling conductance (solid) to the structure observed in the optical conductivity (dashed). Note that the peaks and valleys in both measurements appear at similar frequencies. The Drude contribution has been subtracted from the optical conductivity. The tunneling conductance has been divided by the BCS conductance.

why in Fig. 7 there is such excellent agreement between the tunneling conductance and the optical conductance. The optical results can be understood as arising from a Fano interaction between the continuum electronic states and selected phonon modes leading to a strong suppression of the optical transition probability. The similarity of the tunneling results suggests that the electronic density of states is suppressed at these phonon energies albeit by a small amount. We recognize that to date no solid theoretical basis exists for such a modification and that such structures have not previously been observed in tunneling experiments. We note, however, that this interpretation does account for the agreement between the optical and tunneling data and that it brings both sets of data into excellent accord with the experimentally measured phonon density of states.

There is a means of distinguishing our interpretation of the electron-phonon interaction and a conventional Holstein process if one interprets the tunneling data in terms of a conventional s-wave superconducting gap. In tunneling spectroscopy, it is customary to subtract Δ from the energy scale since a structure due to a phonon of frequency Ω in a strong coupled BCS superconductor appears at energy $\Delta+\Omega$. The agreement between the optical and tunneling conductivity shown in Fig. 7 was obtained without shifting the energy axis even though the tunneling data were obtained from the superconducting state while the optical measurements were taken in the normal state. Within the model that we have used, no shift is anticipated. Such a shift would move the solid curve in Fig. 7 to lower frequencies by 3.7 meV (30 cm^{-1}) which would slightly reduce the quality of the agreement. Clearly a priority will be to measure the phonon features both in the tunneling and optical measurements above and below the transition temperature. Preliminary measurements of the optical properties of $Nd_{1.85}Ce_{0.15}CuO_{4+\delta}$ in the superconducting state show no shift in the phonon structure below T_c. Likewise, if features are visible at temperatures above and below T_c in tunneling data we would expect them to appear at the same energies.

V. CONCLUSIONS

Despite the unique properties exhibited by $Nd_{1.85}Ce_{0.15}CuO_{4+\delta}$, its far-infrared optical spectra appear to exhibit many of the features common to the other cuprate superconductors. These features include the ledge in the reflectance at 420 cm^{-1}, the linear reflectance in the midinfrared, and the development of the midinfrared band as the doping level is increased. Our analysis of the optical conductivity shows that it has two components. The first component can be described in terms of a Drude model with a temperature-dependent scattering rate that closely follows the temperature dependence of the dc resistivity. The second component is relatively insensitive to temperature and has been modeled in terms of phonons which are resonantly coupled to a broad midinfrared band. The phonon structure seen in tunneling experiments by Huang *et al.*[27] is in remarkable agreement in position and relative intensity

with our optical conductivity, which is not expected for a simple Holstein process.

ACKNOWLEDGMENTS

The authors would like to thank Maureen Reedyk and E. L. Wolfe for helpful discussions and John Zasadzinski both for discussions and for making his tunneling conductance available to us. This work was supported by the Ontario Center for Materials Research (OCMR) and the Natural Sciences and Engineering Research Council of Canada (NSERC).

[1]Y. Tokura, H. Takagi, and S. Uchida, Nature **337**, 345 (1989).
[2]H. Tagaki, S. Uchida, and Y. Tokura, Phys. Rev. Lett. **62**, 1197 (1989).
[3]C. C. Tsuei, A. Gupta, and G. Koren, Physica C **161**, 415 (1989).
[4]S. L. Cooper, G. A. Thomas, J. Orenstein, D.H. Rapkine, A. J. Millis, S. Cheong, A. S. Cooper, and Z. Fisk, Phys. Rev. B **41**, 11 605 (1990).
[5]Ji-Guang Zhang, Xiang-Xin Bi, E. McRae, P. C. Eklund, B. C. Sales, and M. Mostoller, Phys. Rev. B **43**, 5389 (1991).
[6]K. Hirochi, S. Hayashi, H. Adachi, T. Mitsuyu, T. Hirao, K. Setsune, and K. Wasa, Physica C **160**, 273 (1989).
[7]S. Lupi, P. Calvani, M. Capizzi, P. Maselli, W. Sadowski, and E. Walker, Phys. Rev. B **45**, 12 470 (1992).
[8]E. V. Abel', V. S. Bagaev, D. N. Basov, O. V. Dolgov, A. F. Plotnikov, A. G. Poiarkov, and W. Sadovsky, Solid State Commun. **79**, 931 (1991).
[9]S. Uchida, T. Ido, H. Takagi, T. Arima, Y. Tokura, and S. Tajima, Phys. Rev. B **43**, 7942 (1991).
[10]Y. Lu, R. A. Hughes, T. Strach, T. Timusk, D. Poulin, and J. S. Preston, Physica C **197**, 75 (1992).
[11]M. Reedyk, D. Bonn, J. D. Garrett, J. E. Greedan, C. V. Stager, T. Timusk, K. Kamarás, and D. B. Tanner, Phys. Rev. B **38**, 11 981 (1988).
[12]C. M. Foster, K. F. Voss, T. W. Hagler, D. Mihailović, A. J. Heeger, M. M. Eddy, W. L. Olson, and E. J. Smith, Solid State Commun. **76**, 651 (1990).
[13]M. Reedyk, T. Timusk, J. S. Xue, and J. E. Greedan, Phys. Rev. B **45**, 7406 (1992).
[14]Z. Schlesinger, R. T. Collins, D. L. Kaiser, and F. Hotzberg, Phys. Rev. Lett. **59**, 1958 (1987).
[15]J. H. Kim, I. Bozovic, J. S. Harris, Jr., W. Y. Lee, C. B. Eom, and T. H. Geballe (unpublished).
[16]S. Tajima, H. Ishii, T. Nakahashi, T. Takagi, S. Uchida, M. Seki, S. Suga, Y. Hidaka, M. Suzuki, T. Murakami, K. Oka, and H. Unoki, J. Opt. Soc. Am. B **6**, 475 (1989).
[17]T. Timusk and D. B. Tanner, Physica C **169**, 425 (1990).
[18]M. J. Rice, Phys. Rev. Lett. **37**, 36 (1976).
[19]T. Holstein, Phys. Rev. **96**, 539 (1954).
[20]R. R. Joyce and P. L. Richards, Phys. Rev. Lett. **24**, 1007 (1970).
[21]B. Farnworth and T. Timusk, Phys. Rev. B **14**, 5119 (1976).
[22]U. Fano, Phys. Rev. **124**, 1866 (1961).
[23]T. Timusk, C. D. Porter, and D. B. Tanner, Phys. Rev. Lett. **66**, 663 (1991).
[24]K. Kamarás, S. L. Herr, C. D. Porter, N. Tache, D. B. Tanner, S. Etemad, T. Vankatesan, E. Chase, A. Inam, X. D. Wu, M. S. Hegde, and B. Dutta, Phys. Rev. Lett. **64**, 84 (1990).
[25]D. B. Romero, C. D. Porter, D. B. Tanner, L. Forro, D. Mandrus, L. Mihaly, G. L. Carr, and G. P. Williams, Phys. Rev. Lett. **68**, 1590 (1992).
[26]J. W. Lynn, I. W. Sumarlin, D. A. Neumann, J. J. Rush, J. L. Peng, and Z. Y. Li, Phys. Rev. Lett. **66**, 919 (1991).
[27]Q. Huang, J. F. Zasadzinski, N. Tralshawala, K. E. Gray, D. G. Hinks, J. L. Peng, and R. L. Greene, Nature **347**, 369 (1990).
[28]E. L. Wolfe, *Principles of Electron Tunneling Spectroscopy* (Oxford University Press, New York, 1985).
[29]P. B. Allen, Phys. Rev. B **3**, 305 (1971).
[30]J. M. Rowell and W. M. McMillan, Phys. Rev. Lett. **16**, 453 (1966).